THE WIDTH OF UNCONFINED SLAB AVALANCHES BASED ON FIELD MEASUREMENTS OF SLAB PROPERTIES

J.B. Jamieson and C.D. Johnston[1]

Using principles of fracture mechanics, a linear elastic model of an unconfined dry slab and simplifying assumptions, expressions are derived for the energy release rate and for the fracture resistance during the propagation of the rapid brittle fractures which release slab avalanches. The simplified energy release rate is constant as the fractures advance whereas the fracture resistance increases as the fractures spread across the slope. The arrest criterion equates the release rate to the resistance and gives an expression for the width of unconfined slab avalanches in terms of two empirical constants and three field measurements, namely the tensile strength of the slab, the slab density and the inclination of the starting zone. The empirical constants are evaluated by regressing the expression for the width of unconfined slab avalanches on data obtained from measurements made at 13 *strictly unconfined* slab avalanches during the winters of 1988 and 1989 in the Rocky Mountains of Western Canada. The significant correlation coefficient (0.81) suggests that the expression may provide a quantitative approach to forecasting the width of unconfined slab avalanches.

FAILURE MODEL OF AN UNCONFINED SLAB

Slab failure (Figure 1) begins with shear failure in the weak layer below the slab (Perla and LaChapelle, 1970; McClung, 1987). Initially, the basal shear failure is ductile (Gubler and Bader, 1989). Following the initial basal failure, rapid brittle fractures propagate in shear on the bed surface and in tension at the crown resulting in an unconfined slab avalanche.

The following analysis considers a laterally unconfined snowpack consisting of slab of constant thickness D and density ρ. The slab overlies a weak basal layer which, in turn, lies on an essentially rigid bed surface inclined at an angle β from the horizontal. The snow slab is modelled as an infinite plate of uniform snow, which under rapid loading, exhibits linearly elastic behaviour and brittle failure. The basal fracture spreads down the slope and equally in both cross-slope directions resulting in crown, flank and stauchwall fractures. The cross-slope width of the slab cut out by the fractures is $2B$ and the distance from the crown to the stauchwall is L.

ENERGY RELEASE

During avalanche release, there are two main sources of energy. As the mass of snow moves downhill, a large amount of potential energy is released, much of which is translated into the kinetic energy of the mass. The other source is the strain energy stored in the

[1]Dept. of Civil Engineering, University of Calgary, Calgary, Canada.

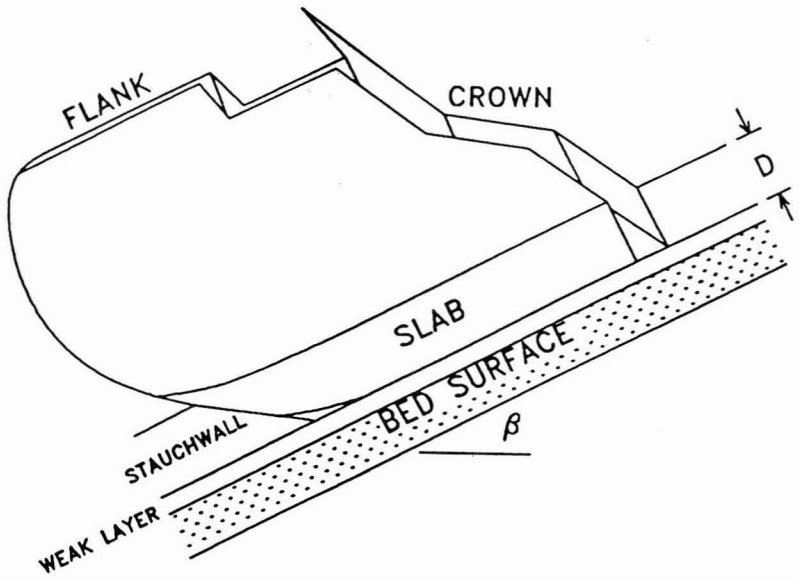

Figure 1: Slab Avalanche Nomenclature

snowpack. Since rapid tensile cracks are occasionally observed that are not followed by avalanche release, we assume that the energy required to propagate the crown fracture is supplied largely by the strain energy of the slab. Since the weak layer below the slab is often very thin (e.g. 1 mm) compared to the slab (0.1 to 4.2 m) (Perla, 1977), the slab is the obvious source of the strain energy to propagate the fractures which release slab avalanches.

As shown in Figures 1 and 2, the weak basal layer fails in shear and the crown fractures in tension. Noting that practical expressions for the energy released by such dynamic mixed-mode fractures in layered materials are not available, we make the following simplifying assumptions:

1. most of the strain energy released is due to the crown fracture, and

2. the energy released by the crown fracture can be approximated by considering the slab ahead of each tip of the crown fracture to be in slope-parallel tension resulting from the basal fracture advancing ahead of the crown fracture.

This slope-parallel tension (Figure 3) is essentially the static stress state considered by Perla and LaChapelle (1970), Brown and others (1972) and by Conway and Abrahamson (1984). The following derivation considers first the strain energy release for the static state and then adapts the derived expression for dynamic effects.

Overlying the failed region of the basal layer, a portion of the slab is supported by the surrounding slab. Slope-parallel compression occurs where the slab is supported from down-slope, and slope-parallel tension occurs where the slab is supported from up-slope. Between the compression zone and the tension zone, there is a point N at which the slope-parallel stress is zero. From statics, the slope-parallel stress in the tension zone a distance x upslope from N is:

$$\sigma_I = \rho g x \sin\beta. \tag{1}$$

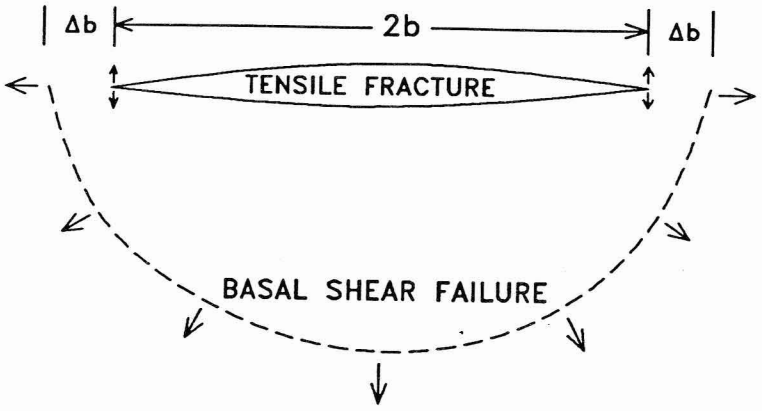

Figure 2: A Model of Advancing Basal and Crown Fractures

If the failed zone is sufficiently large, the crown fracture occurs a distance λ upslope from N where the slope-parallel stress reaches the tensile strength of the slab σ_{slab}. Substituting $\sigma_I = \sigma_{slab}$, Eq. 1 can be solved for $x = \lambda$:

$$\lambda = \frac{\sigma_{slab}}{\rho g \sin \beta}. \tag{2}$$

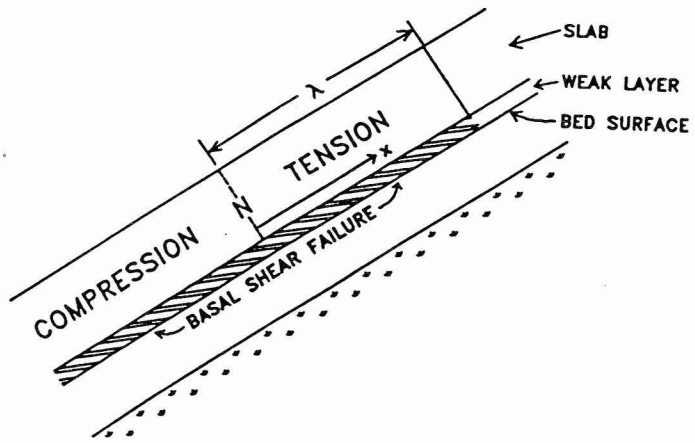

Figure 3: Slab Tension and Compression Zones due to Basal Shear Failure

The slope-parallel stress σ_I in the tensile zone ranges from 0 to σ_{slab}:

$$\sigma_I = \left(\frac{x}{\lambda}\right) \sigma_{slab} \tag{3}$$

and, neglecting Poisson effects, the slope-parallel strain ϵ_r ranges from 0 to the critical elastic strain of the slab ϵ_{slab}:

$$\epsilon_r = \frac{\sigma_I}{E} \tag{4}$$

$$= \left(\frac{x}{\lambda}\right)\frac{\sigma_{slab}}{E} \tag{5}$$

$$= \left(\frac{x}{\lambda}\right)\epsilon_{slab}. \tag{6}$$

in which E is Young's Modulus for the slab.

To calculate the strain energy that will be released from the tension zone, we consider a volume dV of the tensile zone with down-slope length λ, slope-perpendicular thickness D and cross-slope width db. Using Eqs. 1, 2, 3, and 6, the strain energy dU that will be released by the crown fracture advancing a distance db across the top of the tension zone is:

$$dU = \int_V \sigma_I \epsilon_r dV \tag{7}$$

$$= Ddb\int_0^\lambda \left(\frac{x}{\lambda}\sigma_{slab}\right)\left(\frac{x}{\lambda}\epsilon_{slab}\right)dx \tag{8}$$

$$= D\sigma_{slab}\epsilon_{slab}\left(\frac{\lambda}{3}\right)db \tag{9}$$

$$= \frac{D\sigma_{slab}^2\epsilon_{slab}}{3\rho g\sin\beta}db. \tag{10}$$

If the fracture were to advance quasi-statically across the slope, the crown fracture would release energy at a rate:

$$G_{stat} = \frac{dU}{db} \tag{11}$$

$$= \frac{D\sigma_{slab}^2\epsilon_{slab}}{3\rho g\sin\beta} \tag{12}$$

which is constant across the slope.

For a tension crack propagating rapidly through an infinite slab, the energy release rate will be reduced by a dynamic factor k_{dyn} which depends linearly on the speed of the crack tip (Broek, 1982, pp. 147-148), giving an energy release rate of:

$$G = k_{dyn}G_{stat} \tag{13}$$

$$= k_{dyn}\frac{D\sigma_{slab}^2\epsilon_{slab}}{3\rho g\sin\beta}. \tag{14}$$

WORK OF FRACTURE

Work must be done to create two new fracture surfaces in the weak basal layer and at the crown, flanks and stauchwall. The basal fracture is modelled as an expanding semi-ellipse with down-slope length ℓ and cross slope width $2(b+\Delta b)$. Since the area of the bed surface is typically much greater than the surface area of the other fractures (Perla, 1977), the work done to expand the quarter-ellipse on either side of the initial failure can be approximated by the work required to create the two fracture surfaces at the base of the slab:

$$W_f = \frac{\pi}{2}(b+\Delta b)\ell\gamma_{basal} \tag{15}$$

where γ_{basal} is the surface energy (Griffith, 1920) for the weak basal layer. This surface energy depends strongly on the area of the broken ice skeleton and hence on the density of the weak layer.

The final length of ℓ is L and this distance from the crown to stauchwall is difficult to measure because the stauchwall is often eroded by the moving slab. However, Brown and others (1972) report ratios of the crown-to-stauchwall length to the cross-slope fracture width which average 1/2 as shown in Figure 4. Therefore, the simplest plausible expression for ℓ is $b/2$ which is assumed to be constant during the advance of basal fractures.

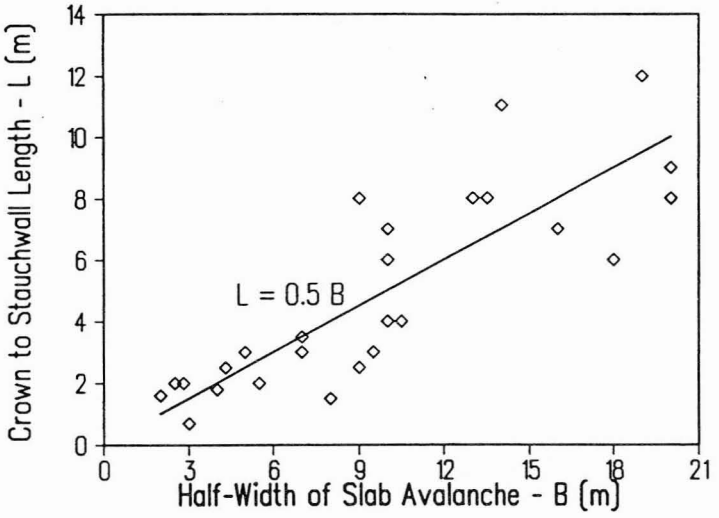

Figure 4: Observed Length and Half-Width of Unconfined Slab Avalanches (Data from Brown and others, 1972)

As the fractures propagate across the slope, the resistance, R, is:

$$R = \frac{dW_f}{db}. \tag{16}$$

Using Eq. 15, $\ell = b/2$ and assuming Δb to be constant, the resistance is:

$$R = \frac{\pi}{4}(2b + \Delta b)\gamma_{basal} \tag{17}$$

The surface energy per unit area, γ_{basal}, of the fractures also needs to be expressed in terms of quantities which can be measured easily in the field. Noting that surface energy is the energy required to make new surfaces of unit area and that tensile strength is the force required to make new surfaces of unit area (Hobbs, 1974, p. 434), we assume proportionality between these two highly density-dependent properties:

$$\gamma_{basal} = k_{\gamma/\sigma}\sigma_{basal} \tag{18}$$

in which $k_{\gamma/\sigma}$ has units of length and is taken to be constant.

The tensile strength of a very thin weak layer cannot be measured in the field. However, McClung (1979) speculates that, for snow, the shear strength may approach the

tensile strength and Jamieson (1989) presents supporting data. Therefore, the fracture resistance can be approximated by:

$$R = \frac{\pi}{4}(2b + \Delta b)k_{\gamma/\sigma}\tau_{basal} \tag{19}$$

in which τ_{basal} is the shear strength of the weak layer.

FRACTURE ARREST

In the preceding sections, expressions for the energy release rate and for the fracture resistance are derived. The energy release rate, G, is constant across the slope unlike the fracture resistance, R, which increases with b. The energy balance for the propagation of the brittle fractures is shown in Figure 5.

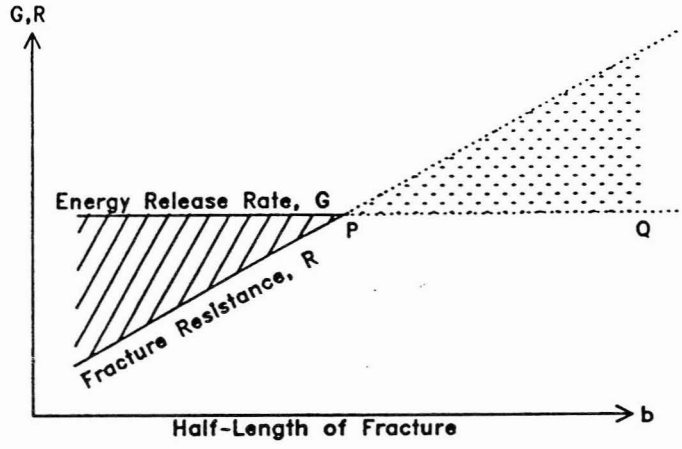

Figure 5: Strain Energy Release Rate and Fracture Resistance During Brittle Propagation

Two criteria for the arrest of the fracture are plausible. Either the fracture stops at $b = P$ when the resistance reaches the rate of energy release or it continues and stops closer to $b = Q$ when:

$$\int_0^P (G - R)db = \int_P^Q (R - G)db \tag{20}$$

Broek (1982, pp. 155-156) notes that P is a more logical arrest point than Q since the surplus energy will likely be in kinetic form which, for a long crack, will lag far behind the crack tip. Assuming the fracture stops at P, the arrest criterion is:

$$R = G \tag{21}$$

Substituting from Eqs. 14 and 19, this is:

$$\frac{\pi}{4}(2B + \Delta b)k_{\gamma/\sigma}\tau_{basal} = k_{dyn}\frac{D\sigma_{slab}^2\epsilon_{slab}}{3\rho g \sin\beta} \tag{22}$$

in which B is the final length of b.

We assume the critical elastic strain ϵ_{slab} is constant since the critical brittle strain is nearly constant (Narita, 1983). Including the constants π, g, $k_{\gamma/\sigma}$, k_{dyn} and ϵ_{slab} into the proportionality constant C and solving for B:

$$B + \frac{\Delta b}{2} = C \frac{D\sigma_{slab}^2}{\tau_{basal}\rho \sin\beta}. \tag{23}$$

Noting that τ_{basal} can be approximated by $\rho g D \sin\beta$ (Perla and others, 1982) and assuming Δb is small compared to B, the arrest criterion becomes:

$$B = C \left(\frac{\sigma_{slab}}{\rho \sin\beta} \right)^2. \tag{24}$$

COMPARISON WITH FIELD MEASUREMENTS

In the Rocky Mountains of Alberta during the winters of 1987-88 and 1988-89, the slab properties, σ_{slab}, ρ and β were measured an average of four times near the crown fractures of each of thirteen slab avalanches. Each of the thirteen avalanches was *strictly unconfined,* that is, neither flank tapered to less than half the mean crown thickness nor did either flank abut rock outcrops or dense timber. The number of crown fractures examined is limited because most avalanches are confined in some way and because of practical difficulties involved in safely accessing crown fractures before properties such as density and tensile strength change substantially.

Mean values of σ_{slab} varied from 0.4 to 3.5 kPa, ρ from 100 to 220 kg m^{-3} and β from 26 to 45°. Also, mean values of D ranged from 0.10 to 0.44 m. These values of ρ and D fall at the low end of the ranges reported by Perla (1977) for slab avalanches. The tensile strength of these slabs, σ_{slab}, was measured by the test method developed by Conway and Abrahamson (1984) and evaluated and described in detail by Jamieson and Johnston (1989).

The proposed avalanche width "predictor", $(\sigma_{slab}/\rho \sin\beta)^2$, is calculated from the mean values of the three variables for each of the slab avalanches. In Figure 6 the relationship between the observed widths of these slab avalanches and $(\sigma_{slab}/\rho \sin\beta)^2$ is approximately linear with a correlation coefficient of 0.81. Different symbols are used to distinguish between avalanches which occurred naturally and those which were triggered by skier or by explosive and there is no apparent influence of the different triggers on the widths of the avalanches.

These thirteen data are regressed on $(\sigma_{slab}/\rho \sin\beta)^2$ giving:

$$2B = 2.2 + 2.0\,(\sigma_{slab}/\rho \sin\beta)^2 \tag{25}$$

in which D is measured in metres, σ_{slab} in Pa and ρ in kg m^{-3}.

This estimating equation gives minimum and maximum values for the widths of slab avalanches which are in approximate agreement with field observations of unconfined slab avalanches. Using a slab density of 60 kg m^{-3}, a corresponding tensile strength of 100 Pa and a slope of 50°, Eq. 25 gives a minimum predicted value for $2B$ of 3 m. Similarily, for a slab density of 400 kg m^{-3}, a corresponding tensile strength of 15 kPa and a slope angle of 25°, Eq. 25 gives a maximum predicted value for $2B$ of 1.5 km.

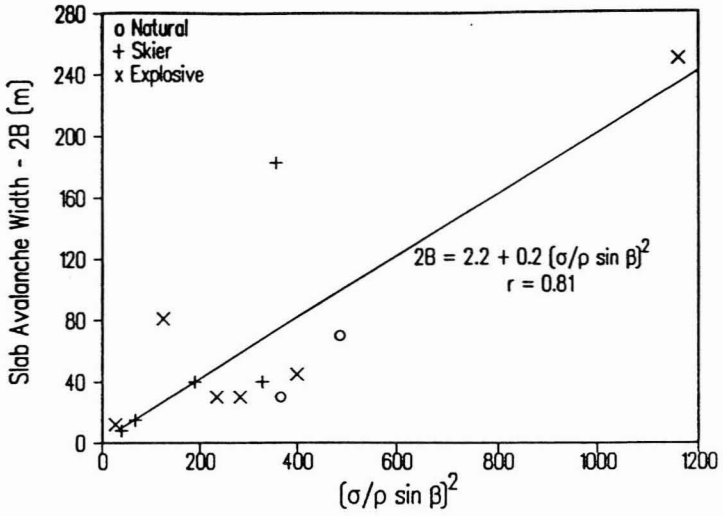

Figure 6: Observed Widths of Slab Avalanches vs $(\sigma_{slab}/\rho \sin\beta)^2$
Values of $(\sigma_{slab}/\rho \sin\beta)^2$ are based on measurements of slab tensile strength, density and slope inclination made near the crown fractures of 13 strictly unconfined slab avalanches in the Canadian Rockies during the winters of 1988 and 1989.

Avalanche widths much greater than predicted by Eq. 25 may be possible if one slab avalanche sympathetically triggers additional slab avalanches and the crown fractures of these avalanches join. The 183 m wide avalanche shown in the upper left portion of Figure 6 may be one such case. It consisted of two arcing crown fractures of width 56 and 107 m separated by a 20 m wide piece of the slab which extended an estimated 30 m down-slope from the neighbouring crown fractures. Five measurements of σ_{slab}, ρ and β were made at each crown, allowing separate values of the predictor to be calculated. Treating this 183 m wide slab avalanche as two separate slab avalanches with widths of 56 and 107 m gives a correlation coefficient of 0.91 for the resulting 14 unconfined slab avalanches.

In addition to the data reported in Figure 6, the measurements σ_{slab}, ρ and β were made at the crown fractures of 4 slab avalanches which did not meet all the criteria required for strictly unconfined avalanches. The widths of each of these avalanches fall below the regression line for strictly unconfined avalanches (Eq. 25) as shown in Figure 7. This supports the criteria included in the definition for strictly unconfined avalanches.

One factor which may limit the application of Eq. 25 is that tensile strength measurements may be impractical for some avalanche control programs. However, for uniform slabs (as opposed to multilayer slabs), the approximate tensile strength of the slab σ^*_{slab} can be estimated from the mean density of the slab. Since most uniform slabs consist of new, partly settled or rounded grains, an appropriate empirical equation (Jamieson and Johnston, 1989) is:

$$\sigma^*_{slab} = 79.7 \left(\frac{\rho}{\rho_{ice}}\right)^{2.39} \tag{26}$$

in which ρ_{ice}=917 kg m^{-3}. Using σ^*_{slab} from this equation for σ_{slab} in Eq. 25 results in predicted values for $2B$ which are based only on slab density and slope inclination. For the

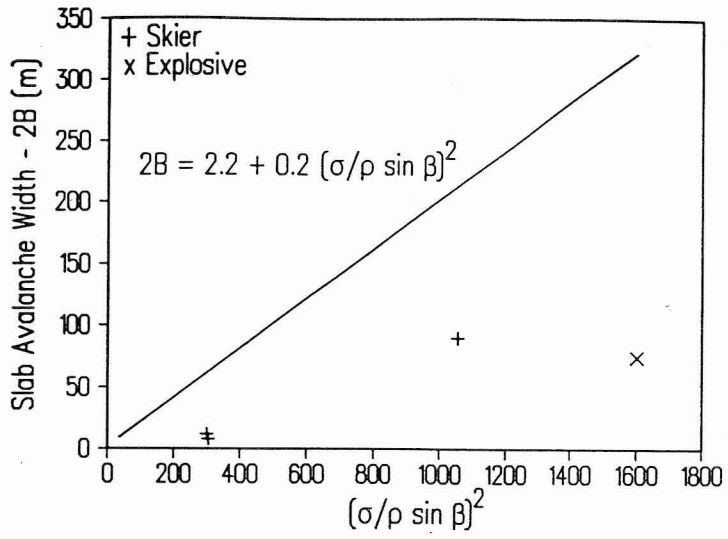

Figure 7: The Width of Four Confined Slab Avalanches Compared to the Regression Line for the Width of Unconfined Slab Avalanches
Values of $(\sigma_{slab}/\rho \sin \beta)^2$ are based on measurements of slab tensile strength, density and slope inclination made near the crown fractures of slab avalanches in the Canadian Rockies. These slab avalanches did not meet all the criteria for strictly unconfined slab avalanches.

13 strictly unconfined slab avalanches discussed previously, observed avalanche widths are plotted against $(\sigma^*_{slab}/\rho \sin \beta)^2$ in Figure 8. The correlation coefficient for the relation between the observed avalanche widths and $(\sigma^*_{slab}/\rho \sin \beta)^2$ is 0.71. This decrease in the correlation coefficient from 0.81 to 0.71 is due to the empirical estimate for the tensile strength of the slab.

A second data set for generally thicker (0.43 to 1.06 m) slab avalanches which occurred between 1979 and 1988 was obtained from Parks Canada. This data set consists of eleven occurrence reports and the corresponding fracture line profiles. Each avalanche was reported to be unconfined and the fracture line profile included density measurements.

The observed widths of these avalanches are also plotted against $(\sigma^*_{slab}/\rho \sin \beta)^2$ in Figure 8. As indicated by the correlation coefficient of 0.09, these data are scattered widely. Two factors may explain the failure of $(\sigma^*_{slab}/\rho \sin \beta)^2$ as a useful indicator of avalanche width for the second data set:

- it is not known if these avalanches meet all the criteria for strictly unconfined slab avalanches, and
- the slabs in the second data set are thicker and all but one consist of multilayer slabs for which Eq. 26 may not provide a reasonable estimate for σ_{slab}.

For operations in which tensile strength measurements are practical, Eq. 25 offers a promising approach to quantitatively forecasting the width of slab avalanches. When tensile strength measurements are not available, Eq. 25 may still prove useful for thin ($D < 0.4$ m) single-layer slabs where the density and grain structure are essentially uniform and can therefore be used to estimate the tensile strength according to Eq. 26. However, more data are required to establish whether these equations are applicable to snowpacks

that are climatically and perhaps structurally quite different from the eastern Rockies snowpack where the experimental data for Figures 6, 7 and 8 were obtained.

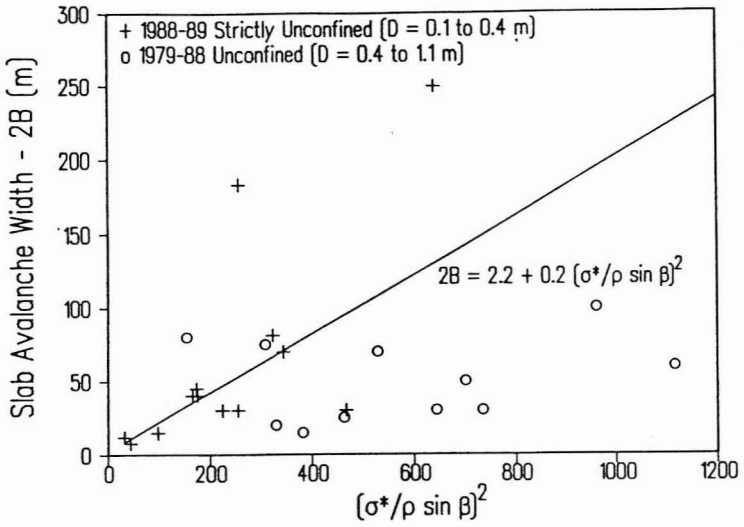

Figure 8: Observed Widths of Slab Avalanches vs $(\sigma^*_{slab}/\rho \sin\beta)^2$
For the 1988-89 data, values of $(\sigma^*_{slab}/\rho \sin\beta)^2$ *are based on measurements of slab density and slope inclination made near the crown fractures of 13 strictly unconfined slab avalanches in the Canadian Rockies. For the 1979-88 data, slab density and slope inclinations are taken from fracture line profiles of unconfined slab avalanches in the Canadian Rockies.*

ACKNOWLEDGEMENTS

Clair Israelson and David Norcross of Environment Canada (Parks) provided advice and assistance as well as the fracture line profile and occurrence reports which made up the second data set. R.I. Perla of the National Hydrology Research Institute and N.G. Shrive of the University of Calgary made useful suggestions regarding the paper. The staff of the Temple Research Station at Lake Louise, John Worrall of Lake Louise Ski Resort and Dave Aikens of Fernie Snow Valley Ski Resort provided assistance. Equipment was loaned by Chris Stethem of Chris Stethem and Associates and R.I. Perla of the National Hydrology Research Institute.

We are grateful to the Natural Sciences and Engineering Research Council (NSERC) and the Alberta Recreation Parks and Wildlife Foundation for financial support.

REFERENCES

BROEK, D. 1982. Elementary Engineering Fracture Mechanics. Martinus Nijhoff, The Hague, 469 pp.

BROWN, C.B., R.J. EVANS and E.R LACHAPELLE. 1972. Slab avalanching and the state of stress of fallen snow. Journal of Geophysical Research, 77(24): 4570-4580.

CONWAY, H. and J. ABRAHAMSON. 1984. Snow stability index. Journal of Glaciology, 30(106): 321-327.

HOBBS, P.V. 1974. Ice Physics. Clarendon, Oxford, 837 pp.

JAMIESON, J.B. 1989. *In situ* tensile strength of snow in relation to slab avalanches. M.Sc. thesis, Department of Civil Engineering, University of Calgary, Calgary, Canada, 142 pp.

JAMIESON, J.B. and C.D. JOHNSTON. 1990. *In situ* tensile tests of snowpack layers. Journal of Glaciology, 36(122): 102-106.

GRIFFITH, A.A. 1920. The phenomena of rupture and flow in solids. Philosophical Transactions of the Royal Society, A(221): 163-198.

GUBLER, H. and H.-P. BADER. 1989. A model of initial failure in slab avalanche release. Annals of Glaciology 13: 90-95.

MCCLUNG, D.M. 1979. *In situ* estimates of the tensile strength of snow utilizing large sample sizes. Journal of Glaciology, 22(87): 321-329.

MCCLUNG, D.M. 1987. Mechanics of snow slab failure from a geotechnical perspective. *In* Avalanche formation, movement and effects, proceedings of the Davos Symposium. International Association of Scientific Hydrology, Publication 162, 475-507.

NARITA, H. 1983. An experimental study on tensile fracture of snow. Contributions from the Institute of Low Temperature Science. Hokkaido University, Sapporo, Japan, Series A 32: 1-37.

PERLA, R.I. 1977. Slab avalanche measurements. Canadian Geotechnical Journal, 14(2): 206-213.

PERLA, R.I. and E.R. LACHAPELLE. 1970. A theory of snow slab failure. Journal of Geophysical Research, 75(36): 7619-7627.

PERLA, R.I., T.M.H. BECK and T.T. CHEUNG. 1982. The shear strength index of alpine snow. Cold Regions Science and Technology, 6: 11-20.